THE MEASUREMENT AND INTERPRETATION OF FLOW WITHIN ROTATING STALL CELLS IN AXIAL COMPRESSORS

I. J. Day† N.A. Cumpsty†

Detailed flow measurements obtained by a new measuring technique are presented for the flow in a stalled axial-flow compressor. Results were obtained from a wide range of compressor builds, including multi-stage and single-stage configurations of various design flow rates and degrees of reaction. Instantaneous recordings of absolute velocity, flow direction and total and static pressures have been included for both full-span and part-span stall.

With the aid of these results, it has been shown that the conventional model of the flow in a stall cell is erroneous. An alternative model is proposed, based on the observation that the fluid must cross from one side of the cell to the other in order to preserve continuity in the tangential direction. An investigation of the experimental results also reveals the finer details of the flow in the cell and shows how these details are related to the design flow rate of the compressor. The influence of these cell details on the power absorbed by a stalled compressor are investigated, and consideration is given to the complex pressure patterns encountered in the compressor.

1 INTRODUCTION

Whereas the literature on rotating stall is extensive, most of it is concerned with stall inception rather than with the flow mechanism once stall is established. There is, however, a real practical need for a better understanding of rotating stall, partly because most multi-stage machines operate under certain conditions with several rows stalled, but also because the behaviour in stall determines the procedures necessary to unstall the machine.

The emphasis on stall inception is particularly true of theoretical studies. In part, this is because the theoretical methods are generally well suited to the considerations of stall inception, since this condition may be identified with the growth of small (i.e. linear) disturbances. It is only recently that Takata and Nagano (**1**)‡ have computed a nonlinear stability analysis.

Consideration of the stall cell has in the past assumed what will be called here a 'dead wake'. The cell is assumed to consist of a region of very low or zero through-flow velocity fluid bounded on either side by streamlines of the unstalled flow. For example, Stenning and Kriebel (**2**) represented stall by vortex sheets along the edges of the cell which produce zero flow within the cell itself. More recently, Fabri (**3**) has proposed a stall model with a dead wake which includes the radial equilibrium condition for the cell, the only model to include this. Both the Stenning and Kriebel and the Fabri models, which are two of the very few concerned with the cell itself, are appropriate only for isolated blade rows; they do not permit the modelling of the multi-stage machines considered here.

There have been a considerable number of experimental studies of stalled compressors, but relatively few have used fast-response instrumentation to examine the details of the cell. Some measurements were reported in the early 1960s by Dunham (**4**), Bodeen (**5**) and Pavlenko (**6**) in Britain, the U.S.A. and the U.S.S.R. respectively, but little followed this until Tanaka and Murata's (**7**) work on a single rotor row in 1975.

Between 1960 and the present day there have been large improvements in instrumentation. In the early 1960s, the interpretation of hot-wire or pressure-transducer data entailed the endless study of paper traces; now, however, the entire operation can be handled by a computer operating in real time. Moreover, the use of a dedicated computer allows ensemble averaging to be employed, with corresponding gains in definition of stall cell properties. This technique, which is the basis of the present paper, has been described elsewhere by Day (**8**)(**9**), but for completeness is outlined in the next section.

The present study was mainly confined to full-span stall, although some studies of part-span stall were made. The ensemble averaging technique can only be used when the disturbance under consideration is repetitive. Full-span stall cells usually satisfy this requirement, but in the case of part-span cells, modulation in cell speed frequently prevents this technique from being used.

All the present results were taken on a low-speed, high hub–tip ratio machine described in the next section. The compressor design was such that by changing the blades a range of different aerodynamic designs could be used, including both isolated rotor and multi-stage builds from one to four stages. Most of the results reported here were obtained from three stage builds of 50 per cent reaction. This choice was made for two reasons. Firstly, there is very little in the way of literature on rotating stall in multi-stage machines and, secondly, because experiments reported in (**9**) show that the performance of a single-stage compressor can differ quite markedly from that of a multi-stage machine. The overall performance of the compressor builds has been described in detail by Day (**9**) and Day, Greitzer and Cumpsty (**10**), and will not be dealt with here where the details of the cell are of prime concern. One aspect should be pointed out, however, and this is that the same machine can develop either part-span or full-span stall. The precise circumstances which produce these types of stall are complicated and described in the above two references; the widely held view that part-span and full-span are the modes for low and high hub–tip ratio machines is either wrong or else is a gross over-simplification.

The MS. of this paper was received at the Institution on 22nd June 1977 and accepted for publication on 15th November 1977.

† *Department of Engineering, University of Cambridge.*

‡ *References are given in the Appendix.*

1.1 Notation

A Flow area
$C_x C_\theta$ Axial and absolute circumferential velocities
$\bar{C}_x$ Axial velocity averaged over annulus area
$\bar{C}_\theta$ Absolute circumferential velocity at centre of stall cell averaged over axial gaps
p Static pressure
p_0 Atmospheric pressure
R_m Radius at annulus mean height
$\bar{U}$ Blade speed at mean radius
λ Fraction of stall cell with reverse axial flow
ρ Density
τ Torque
ϕ Flow coefficient $(=C_x/\bar{U})$
$\bar{\phi}$ Mean flow coefficient $(=\bar{C}_x/\bar{U})$
ϕ^* Design flow coefficient $(=(C_x/\bar{U})_{design})$

2 APPARATUS AND TECHNIQUE

Fig. 1 shows a cross-section through the compressor in a four-stage build. The numbers refer to instrument planes, with even numbers denoting planes upstream of rotors. The drive shaft can be seen passing through the intake from a motor giving a constant speed of 3000 rev min. The tip diameter is 356 mm. A throttle is provided downstream of the exhaust diffuser, and mass flow in unstalled operation is deduced from inlet static pressure. When stalled it is necessary to fit a plenum and orifice plate downstream of the compressor.

Inlet guide vanes are fitted upstream of the first rotor row, so that the stages can be set up to be identical, and outlet guides are present to remove the downstream swirl. The range of builds tested is illustrated by Table 1. The blades were untwisted, which was acceptable in view of the hub–tip ratio of 0.8. The blade chord is 17.8 mm, giving Reynolds numbers, based on chord, of about 0.5×10^5. The various builds are usually referred to by their design flow coefficients, $\phi^* = (C_x/\bar{U})_{design}$, the one exception being the high reaction machine (65 per cent), which was built from the rotor and stator rows of the intermediate and high ϕ^* builds respectively.

The provision for traversing between blade rows meant that there are relatively large axial gaps between them, typically one chord. For one particular build of the low ϕ^* compressor it was possible to run with almost no axial clearance; this was only possible because of the high stagger of this build.

The study of stall cell behaviour hinged on the use of fast-response transducers. The majority of measurements were taken with either a miniature hot-wire (the wire being normal to the radius) or with a cylindrical probe containing a pressure transducer and capable of measuring the instantaneous total pressure. Both of these devices

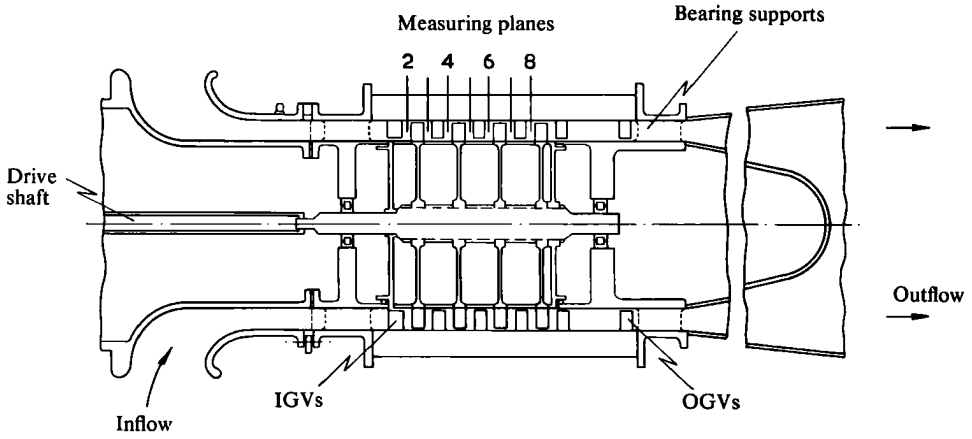

Fig. 1. Cross-section through compressor, showing four-stage build

Table 1. Compressor design parameters

Compressor	No. of stages	Design flow coeff., ϕ^*	Design reaction (per cent)	Stagger angle (rotor/stator)	Camber angle (rotor/stator)
Low ϕ^*	1 3	0.35 0.35	50 50	50°/50°	20°/20°
Intermediate ϕ^*	1 2 3 4	0.55 0.55 0.55 0.55	50 50 50 50	35°/35°	20°/20°
High reaction	1 2 3	0.71 0.71 0.71	65 65 65	35°/20°	20°/40°
High ϕ^*	1 2 3 4	1.0 1.0 1.0 1.0	50 50 50 50	20°/20°	40°/40°

gave outputs dependent on the local flow direction. In addition, transducers capable of measuring static pressure at the wall were used. The dependence of the hot-wire or total pressure probe output on direction was a major complication that was overcome here, but has been neglected in the past. It must be realized that the flow direction can change by as much as 300° when a stall cell passes, and no calibration relying on small variations about a mean would be suitable.

The measurement relied heavily on ensemble (or phase-locked) averaging, and this technique and its precise application here has already been described by Day **(8)(9)**. A stationary probe output is sampled 256 times each time the stall cell passes. The start of sampling is initiated by a separate probe, which in this case was constructed from a ceramic, stereo pick-up cartridge. This small device was fitted upstream of the first rotor row just protruding from the wall and aligned to give a large repeating signal for each passage of the cell.

The results of many cell passages, typically 25, were then ensemble averaged, that is to say, the discrete values at each particular part of the stall cell were added and divided by the number of records taken. The sampling and averaging of the data were accomplished by the computer and, in this way, uncertainty due to unsteadiness, turbulence and noise could be removed. The error due to the directional sensitivity of the hot-wire or total pressure probe remained.

The effect of direction changes were removed using a method that would have been quite impossible without a computer. With any orientation of the probe, the ensemble average will give an accurate measure only when the flow happens to be properly aligned with the probe. At all other flow angles, the device will underestimate the true value. At mechanical arrangement was therefore made so that the probes could be rotated in increments of 10°. In this way, the hot-wire was rotated step-wise through 180°, and the total pressure probe through 360°; the data obtained from each orientation being stored by the computer. (The response of the hot-wire is the same for flows 180° apart; this led to some ambiguity in determining the flow direction, which was resolved with the total pressure probe.) The computer then compared the ensemble average records at each probe angle to determine the maximum value at each point on the stall cell record. From this the correct flow angle and velocity, or total pressure, at each point around the annulus could be determined. The results displayed in this paper consist of the individual points plotted directly by the computer†. Whilst the velocity or pressure magnitudes were measured accurately, the directions could not, of course, be obtained better than to within ±5°. The choice of 10° increments was a compromise between time and precision, but in general this was believed to be adequate in view of the unsteadiness of the flow.

3 RESULTS

3.1 Preliminary tests

A large number of compressor builds were investigated, as Table 1 shows, and as a first step the overall, time mean

† *The results as plotted by the computer and shown in Figs 3–7 therefore correspond to velocity, direction or pressure versus time. The direction of cell movement implied by these figures is therefore from right to left.*

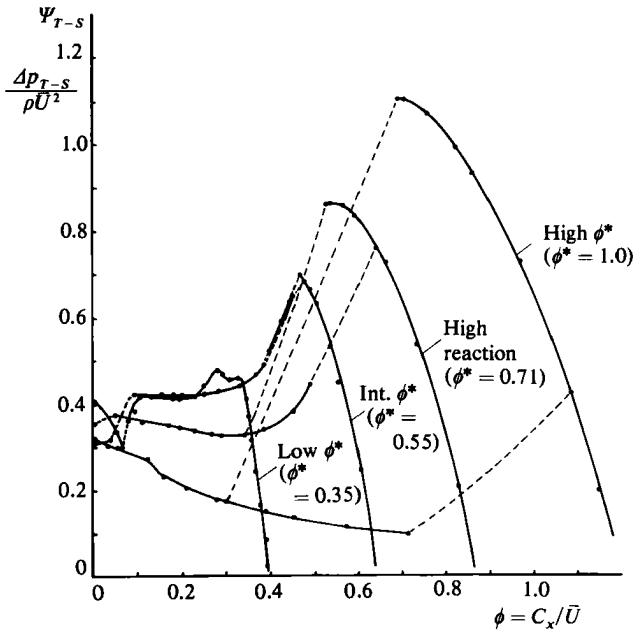

Fig. 2. Total-to-static characteristics of four three-stage builds of different design

pressure characteristics were obtained. These have been reported elsewhere, notably by Day **(9)** and Day, Greitzer and Cumpsty **(10)**, and will not be considered in any detail here. Fig. 2, however, shows the measured total-to-static characteristics of four builds of three-stage compressor, the low, intermediate and high flow coefficient builds of 50 per cent reaction and the one build with 65 per cent reaction. The results are notable for the large variation in unstalled behaviour, but the comparatively similar stalled behaviour, particularly as the flow tends to zero. Results, not shown here, were also obtained for one-, two- and four-stage builds, and in general the results were similar in all cases. As mentioned previously, the single-stage results showed some variations. A test on the three-stage low ϕ^* compressor with reduced axial spacing between rotors and stators showed a change in stalled and unstalled pressure rise, but it was found that the detailed character of the stall cell remained unchanged.

Preliminary tests were also carried out to measure stall cell speed and to determine the type of stall which occurred. As Table 2 shows, the compressor could stall in either part-span or full-span mode, there being a marked tendency for part-span stall to be most common for builds with only one or two stages and low values of the design flow coefficient, ϕ^*. An explanation for this is given in Day *et al.* **(10)**. It will also be seen from Table 2 that the stall cell speed varies widely, depending on the build, being as high as 66 per cent and as low as 11 per cent of blade speed. The part-span stall cells generally rotate at higher speeds than full-span cells, but no explanation for this variation has been found.

The majority of the results presented here are of full-span stall, a few part-span results are shown towards the end to demonstrate the similarity. Furthermore, most of the results are taken from three-stage compressors.

3.2 Velocity measurements

Fig. 3 shows measurements of the instantaneous absolute velocity made with a hot-wire at various stations in three

Table 2. Stall cell details

Compressor	No. of stages	No. of cells	Type of cells	Speed of rotation (expressed as percentage of rotor speed)
Low ϕ^*	1	6 12 1	Part-span Part-span Part-span	31 66 19
	3	4 12 1	Part-span Part-span Full-span	40 60 32
	3 (Reduced spacing)	1 5 1	Part-span Part-span Full-span	29 54 27
Intermediate ϕ^*	1	1 1	Part span Full-span	23 15
	2	1 1	Part-span Full-span	33 22
	3	1 1	Part-span Full-span	41 26
	4	1 1	Part-span Full-span	43 31
High reaction	1	1 1	Part-span Full-span	25 14
	2 3	1 1	Full-span Full-span	24 30
High ϕ^*	1	1 1	Part-span Full-span	24 11
	2 3 4	1 1 1	Full-span Full-span Full-span	20 24 28

Note. Full-span stall cell speeds measured when cell occupied 50 per cent of annulus.

builds of compressor, each with repeating stages. The three compressor builds are of 50 per cent reaction and differ in the design value of flow coefficient, ϕ^*.

The measurements are made between blade rows, the even-numbered measuring planes are ahead of the rotors whilst the odd-numbered planes are behind the rotors. All these measurements were made approximately one third of the annulus height in from the outer wall.

A deliberate choice was made to show so much information on Fig. 3; it allows the similarities from stage to stage to be seen, and it also brings out the similarities between the different compressor builds. Fixing attention on either the stalled or unstalled region of flow for each compressor, it is clear that conditions repeat very closely from stage to stage, despite there being striking differences across each rotor for the flow in the stall cell. This repeatability means that in subsequent figures it is possible to show only the first stage results since the following stages are so similar.

Although the first stage flow is very similar to that in the later stages, and this was found to be true for compressors with two or more stages, the flow in stalled single-stage compressors was rather different. This is discussed in more detail by Day (**9**).

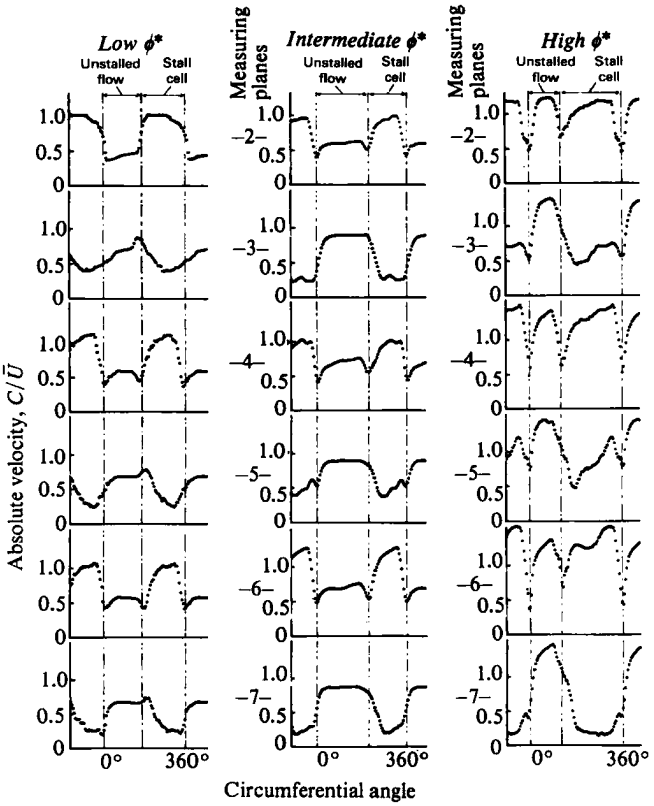

Fig. 3. Absolute velocity in three three-stage compressor builds. $\phi_{test} = 0.20, 0.33, 0.30$ respectively

For all three values of ϕ^*, the absolute velocity in the stall cell is high ahead of the rotor, but low behind it. In each case, the highest absolute velocity is of the order of the blade speed.

The traces in Fig. 3 have all been aligned from the same reference probe, and the vertical broken lines show that the stall cell runs axially through the compressor. This, it will be shown, has important consequences for the stall cell model.

3.3 Flow direction

Fig. 4 shows the instantaneous flow directions upstream and downstream of the first stage rotor corresponding to the velocity measurements in Fig. 3. Because the velocity measurements indicated that stalled flow patterns repeat from stage to stage, it is only necessary to show results for the one stage. These measurements, like those of Fig. 3, were made at one third of the annulus height in from the outer wall. Ahead of the rotor, measuring plane 2, the behaviour is very similar for all three compressor designs and in each case the flow direction is approximately 90° in the stall cell, indicating circumferential flow in the same direction as the rotor. Downstream of the rotor, the situation differs dramatically for the different values of ϕ^*. At low ϕ^*, the flow direction in the cell is similar to that in the unstalled flow. At the intermediate ϕ^*, the flow direction changes about half way across the cell from a value near to the unstalled value up to nearly 270°. (A flow at 270° is tangential, but in the opposite sense to the rotor.) At high ϕ^*, the flow is at approximately 270° across the greater part of the cell.

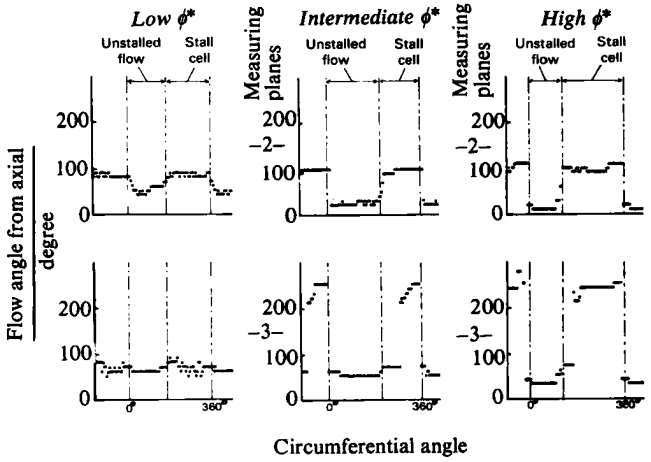

Fig. 4. Flow direction measurements in three compressor builds

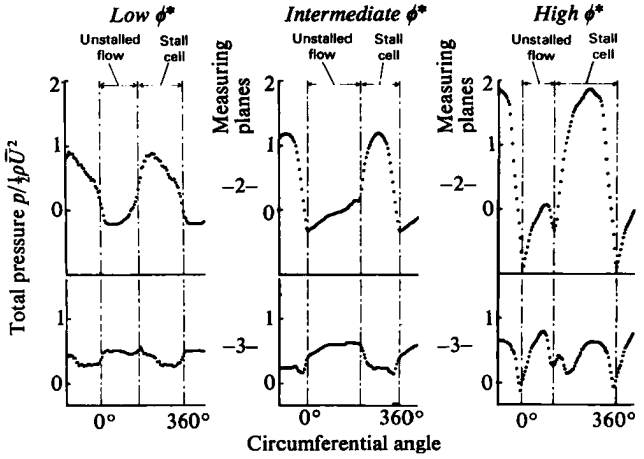

Fig. 5. Total pressure measurements in three compressor builds

3.4 Pressure

The variation in total pressure at the same radial position as those of the previous figures is shown in Fig. 5. This shows very large circumferential variations in total pressure ahead of the rotor and, in particular, relatively larger values in the stall cell for the high ϕ^* build.

The corresponding outer wall static-pressure variation is shown in Fig. 6. In comparative terms, the positive pressures on the outer wall in the stall cell are similar for the three builds. The large variation in the unstalled flow is merely a consequence of the pressure drop for the different local dynamic heads. Clearly, measurement of such pressures with a manometer could give quite misleading results.

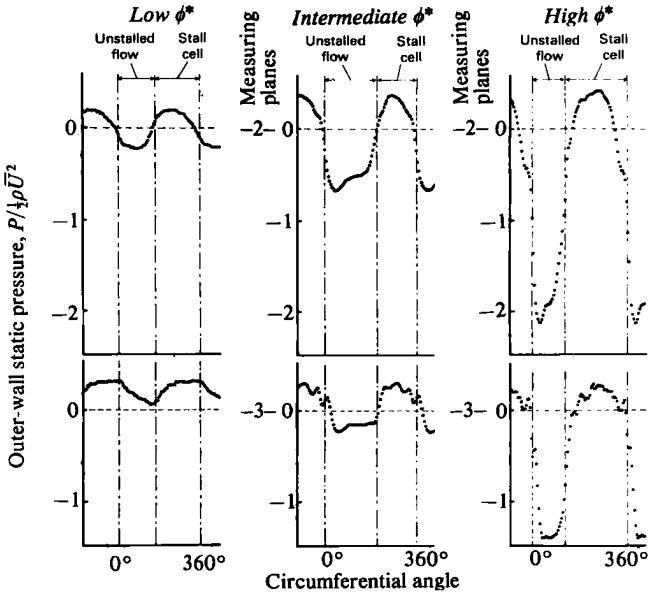

Fig. 6. Outer-wall static pressures before and after the first rotor in three compressor builds

3.5 Effect of cell size

The comparisons of cell behaviour presented so far have ignored the relative size of the stall cell. As Fig. 7 shows, this is justified by the similarity in the behaviour of both the stall cell and unstalled flow as the cell size varies. It is evident that changing the mass flow over a very wide range changes only the proportions of stalled and unstalled flow without altering the fundamental values of either very much.

3.6 Radial variations

Results such as those shown in Figs 3–6 have been obtained at five different radial positions. From these the conditions at the circumferential centre of the cell have been abstracted, and the absolute velocities and flow directions are shown in Figs 8 and 9 respectively, with the solid symbols denoting conditions upstream of the rotor and the hollow symbols downstream.

The velocity measurements show a difference in the variation with radius for builds with different design flow coefficient; the velocities are not only significantly greater for the high ϕ^* machine, actually equal to about 1.2 times blade speed, but the high value extends over more of the annulus.

More dramatic changes with ϕ^* are shown in the flow direction measurements, Fig. 9. For the low ϕ^* machine, the angles on either side of the rotor are similar; in particular, the swirl is in the same sense as the rotor. For the intermediate and high ϕ^* builds, the flow is virtually circumferential ahead of the rotor, with a small negative axial component towards the tip and hub respectively. It is behind the rotor that the large differences are seen for these two builds. For the intermediate ϕ^* build, the variation is complicated, with reverse axial components near the hub and a large swirl in the opposite sense to the rotor. The high ϕ^* build shows a more gradual variation, with a large whirl in the opposite sense to the rotor at all radii. The angular resolution is only good to $\pm 5°$, but it appears to indicate a small reverse axial flow near the tip and positive axial flow near the hub. The measurements of flow angle have been used to calculate the whirl velocities and these are shown as broken lines in Fig. 8.

From the measurements of total pressure (with a pressure transducer) and velocity (with a hot-wire), it is possible to deduce local static pressure. The static pressures at the centre of the stall cell obtained in this way are shown at a number of radii in Fig. 10. Wall static pressures measured directly are shown with a cross, and generally good agreement is evident. The rather less satisfactory agreement in the high ϕ^* case is probably attributable to underestimating the value of velocity from the hot-wire

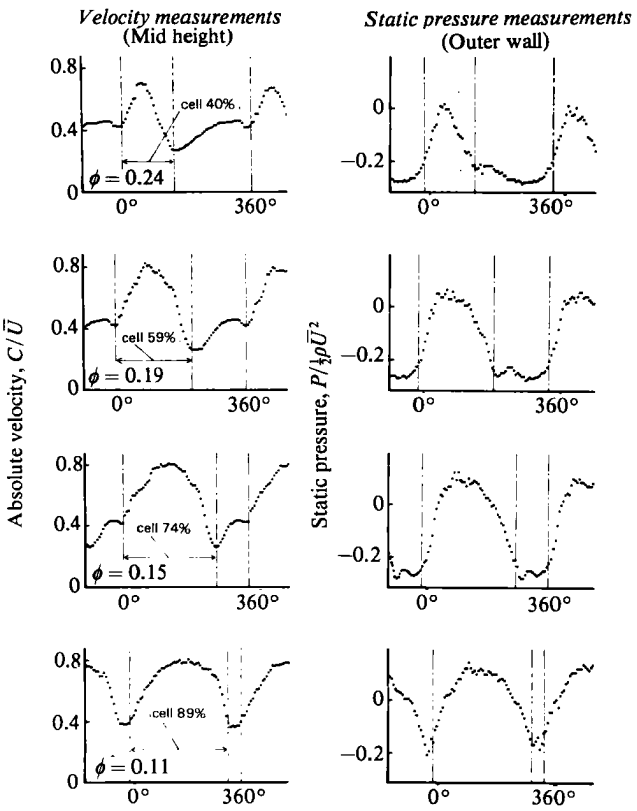

Fig. 7. Velocity and static pressure measurements, showing changes in cell size with decrease in compressor flow rate (Measured ahead of first rotor in a three-stage, low ϕ*compressor)

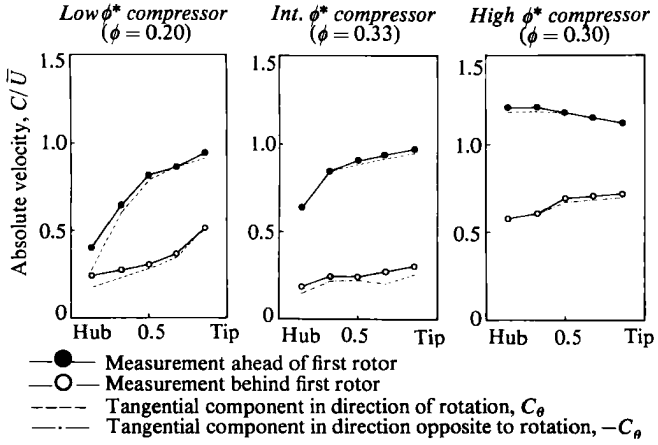

Fig. 8. Absolute velocity at circumferential centre of stall cell in three-stage compressor builds

because of the high temperature in the stall cell. The agreement between the results gives some confidence in the accuracy of the measurements.

3.7 Part-span stall

The results shown in Figs 3–10 were for full-span stall, while those shown in Figs 11 and 12 are for a case of part-span stall occurring in a two-stage build of the intermediate ϕ* compressor. Although conditions are not entirely uniform near the root, the disturbances are very much smaller than those in the cell towards the tip. Just as for full-span stall, a high velocity, high total pressure flow, in essentially the circumferential direction, is found inside the cell ahead of the rotor, Fig. 11. Likewise, the velocity and total pressure are low in the cell downstream of the

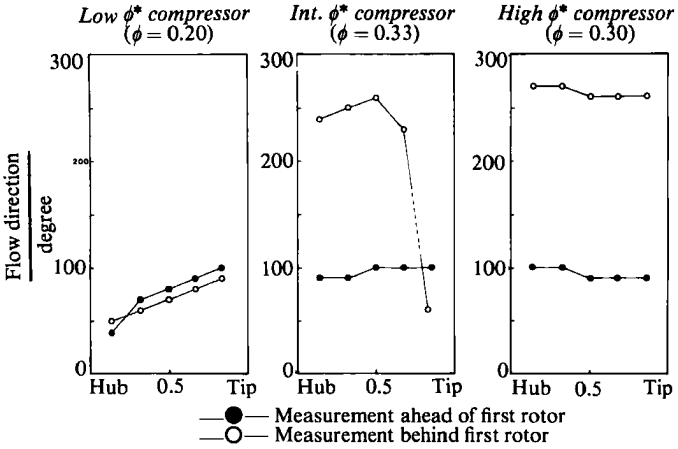

Fig. 9. Flow direction at circumferential centre of stall cell in three-stage compressor builds

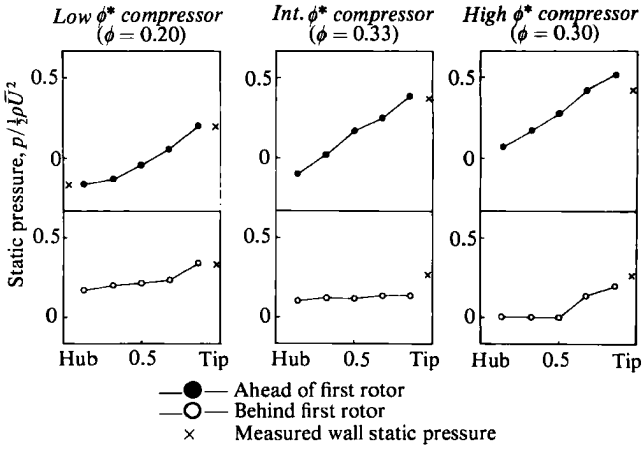

Fig. 10. Static pressure in stall cell calculated from velocity and total pressure measurements in three-stage compressor builds

rotor, Fig. 12. The flow in a part-span cell therefore appears to be similar in nature to that in a full-span stall cell.

4 DISCUSSION OF EXPERIMENTAL RESULTS

4.1 Stall cell structure

From the velocity and flow direction measurements presented in the previous section, a number of general observations can be made about the flow in a stalled compressor. It is clear that in most cases the flow can be divided into distinct areas of stalled and unstalled flow. In the unstalled area, the flow appears to behave as it would if there were no stall cell in the compressor at all. In the stalled area, on the other hand, the results suggest a basic structure to the flow which is responsible for the measurements from each compressor build being generally similar. In this respect, it was found that ahead of the rotors the velocities in the stall cell were consistently near blade speed, and always in the direction of rotation. Behind the rotors, the velocities were much lower by comparison and less predictable in direction. This pattern of high velocities ahead of the rotors and low velocities behind was observed in all the compressor builds, and in the multi-stage configurations gave rise to a cell profile that was invariably found to be axial.

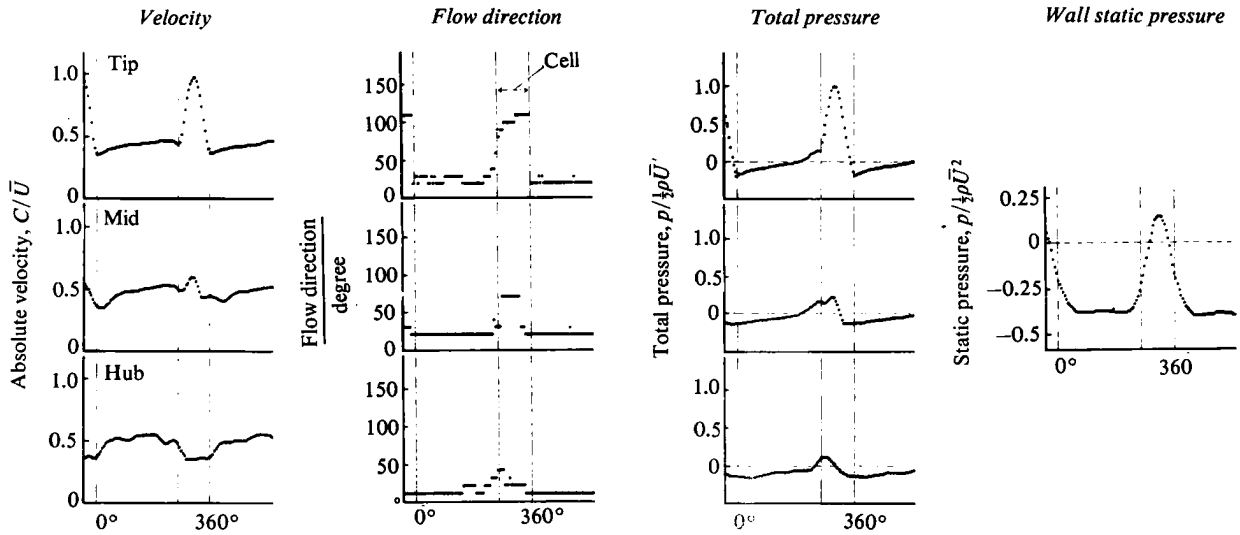

Fig. 11. Part-span stall measurements at three radial positions *ahead of* first rotor in a two-stage intermediate ϕ^* compressor

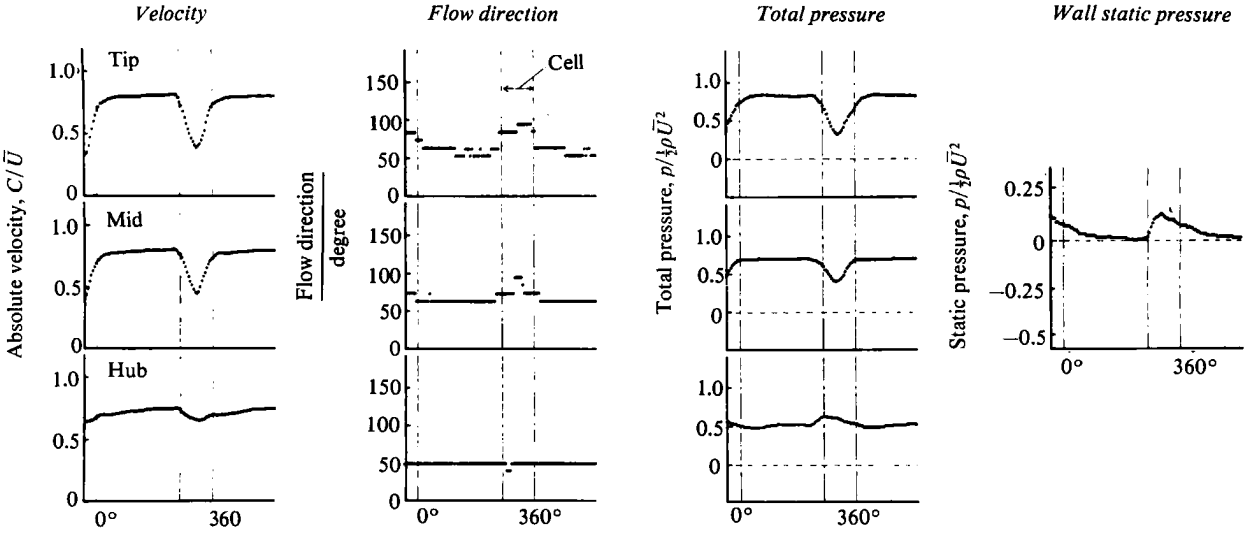

Fig. 12. Part-span stall measurements at three radial positions *behind* first rotor in a two-stage intermediate ϕ^* compressor

The fact that the stall cell extends axially through the multi-stage compressors has been verified by numerous measurements, apart from those presented in Fig. 3. This observation is surprising in view of the conventional idea of stall cell structure. In the past, it has generally been assumed that the stall cell may be viewed as a passive or inactive region of dead fluid, which extends through the blade rows like the wake of a bluff body. Under these conditions, the edges of the cell would coincide with streamlines in the unstalled flow surrounding the cell. The present measurements show, however, that the speed of the cell in all the multi-stage builds is such that, for the edges of the cell to form streamlines in the unstalled flow, the cell would need to assume an obvious helical twist. The consistent recording of high tangential velocities in the stalled region, and the fact that the cell does not exhibit this helical twist, suggest that the cell structure cannot be like that of a dead wake, and, therefore, some alternative structure must be considered. Fig. 13 serves to illustrate the conventional or passive cell structure and introduces the new or active model being considered.

In the unstalled flow surrounding the cell, the mean flow has an average component in the tangential direction which, for a 50 per cent reaction compressor, is always equal to half the mean blade speed, i.e. $0.5\bar{U}$. In the absolute frame of reference, the unstalled flow thus had a component of movement in the same direction as that of the stall cell. It follows that, if the speed of the cell is equal to 50 per cent of the rotor speed, there will be no overall interaction between the stalled and unstalled parts of the flow. If, on the other hand, the stall cell is moving at a lower speed, say 30 per cent (which is roughly the case in all the three-stage builds), the unstalled flow will be moving faster than the stall cell, and fluid will have to cross from one side of the stalled region to the other in order to preserve continuity in the tangential direction.

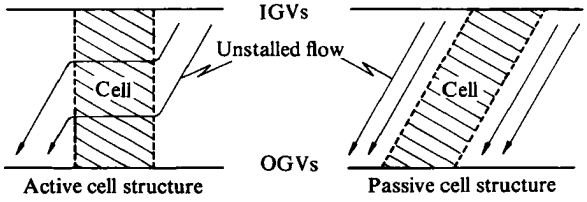

Fig. 13. Comparison of active and passive stall cells

This simple argument, based on the axial profile of the cell and the relative speeds of the stalled and unstalled parts of the flow, gives rise to a picture of the flow in the compressor which can be illustrated by Fig. 14. This sketch is drawn in the absolute reference frame and shows a slow-moving cell ($V_{cell} < 0.5\bar{U}$), in which unstalled flow crosses the cell from one side to the other. (Axial drift in the cell is not included in the figure, which is only intended to illustrate tangential movement.) Before examining the unsteady measurements for further support of this type of flow structure, the question of mass transfer across the stalled region should be considered in greater detail. In the classical article by Rannie (**11**), it was suggested that mass transfer into and out of the cell was an 'unlikely result', and it is therefore important not only to establish the feasibility of such flow, but also to determine what behavioural characteristics might be expected of a cell with this type of structure.

It is helpful to consider an idealized compressor of 50 per cent reaction, in which the stall cell extends axially through the blade rows. The rotor and stator blade chord lengths are assumed equal, and the gaps between the blade rows are provisionally taken to be infinitesimally small. If it is assumed that there is no axial movement of the fluid within the stall cell, then, under ideal conditions, the flow trapped in the stator blade passages will be stationary, while the flow in the rotor blades will be transported in the tangential direction at blade speed, i.e. $\bar{U}$. As the axial projection of the rotor blades occupies half the cross-sectional flow area in the meridional plane, A, the net mass of the fluid being transported tangentially in the stall cell at any instant is given by $\frac{1}{2}\rho A\,\bar{U}$. In the unstalled flow, on the other hand, the mean tangential velocity in a 50 per cent reaction compressor is $0.5\bar{U}$ over the entire flow area, and so the mass being transported circumferentially in this region is also $\frac{1}{2}\rho A\,\bar{U}$. In terms of tangential continuity, therefore, the stalled and unstalled flow régimes are entirely compatible and the concept of an axial cell structure is physically plausible. Furthermore, within the idealization, compatibility of the two tangential flows is independent of the speed of rotation of the cell.

If the idealized compressor is now expanded in the axial direction to create gaps of finite size, the area in the stall cell available for tangential mass transfer will be increased. At the same time, the length of the cell boundaries will be increased proportionately, thus allowing more fluid to enter the cell. If the stalled and unstalled parts of the flow are to remain compatible and the cell to retain its axial orientation, then the area-averaged tangential velocity of the fluid in the gaps between the blade rows in the cell must be equal to $0.5\bar{U}$ for a 50 per cent reaction compressor.

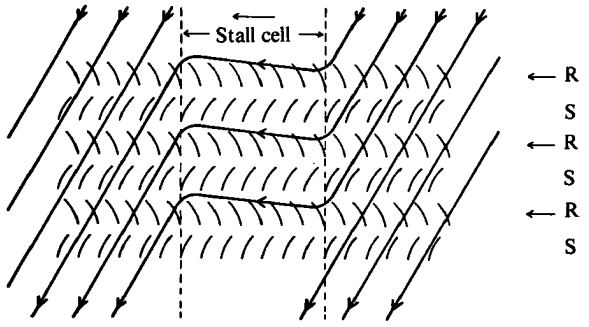

Fig. 14. Sketch of stall cell structure, showing unstalled flow being transported across the cell by the rotor blades (Sketch drawn in absolute reference frame)

The results in Fig. 8 give the tangential components of velocity at the circumferential centre of the stall cell, measured at five radial positions before and after the first rotor in the three-stage compressor builds. (As the flow patterns in a multi-stage compressor have been shown to repeat stage-by-stage, it will suffice to examine the flow in the first stage only.) These results are at the axial position midway between blade rows, but tests suggest that the axial variation in velocity across the gaps is small, and therefore the velocities in Fig. 8 can be taken to represent the mean velocity of the flow between the blade rows. By graphical integration of the measurements before and after the rotor, the following area-averaged velocities were obtained for the tangential flow in the three compressor builds:

Low ϕ^*	$\bar{C}_\theta = 0.51\bar{U}$
Intermediate ϕ^*	$\bar{C}_\theta = 0.54\bar{U}$
High ϕ^*	$\bar{C}_\theta = 0.49\bar{U}$

In each case, the mean velocity is approximately $0.5\bar{U}$. Since the velocity of the stall cell itself is only $0.3\bar{U}$, these measurements firmly establish the existence of tangential flow through the cell, and provide convincing support for the concept of an active cell structure.

It is of interest to note that, while the fluid crossing the stall cell might well do so in both the gaps before and after the rotor, the experimental results show quite clearly that by far the greater movement takes place in the gap ahead of the rotor. The fluid in the gap behind the rotor is inactive by comparison. It appears that any high-velocity fluid drifting out of the stalled rotor blades always does so on the upstream side. Similar observations can be made in compressors of widely different designs (**4**)(**6**)(**7**). Centrifugal effects in the blade passages and local pressure gradients may be partly responsible for this, but, until a suitable explanation for the apparent upstream bias is found, it will not be possible to make any real progress towards predicting the compressor performance from first principles. The influence of blade row spacing was investigated when a special build of the three-stage low ϕ^* compressor was tested with greatly reduced spacing. The results of this experiment show that, apart from a small change in the radial shape, the basic structure of the cell was unaffected by the change in gap/chord ratio.

If the camber angle and chord length of the rotor and stator blades are held equal, but the stagger of one of the blade rows is altered to change the reaction of the compressor, the axial projections of the rotor blade chord lengths is altered. An increase in design reaction reduces the cross-sectional area available for tangential transport of the fluid in the stall cell, but, from the velocity triangles, it can be seen that with an increase in reaction beyond 50 per cent, the mean tangential component of the absolute velocity is reduced below $0.5\bar{U}$. The changes that occur in the stalled and unstalled areas are therefore complementary and, over a limited range, a change in design reaction is not likely to produce any noticeable change in overall cell structure. Indeed, in the current series of tests, when the reaction was raised to 65 per cent by increasing the rotor stagger, the cell structure was unaffected and, in particular, the cell boundaries remained axial. If, on the

other hand, the rotor and stator blades are of markedly different chord lengths, the mass transport capabilities of the stalled rotor and of the unstalled flow do not automatically match. It is then necessary for the cell to assume a helical twist, unless it can adopt a speed equal to the tangential speed of the unstalled flow.

A corollary of the concept of an active cell structure is that the inclination of the cell profile, which is axial in the present series of tests, is independent of the speed of rotation of the cell. It is not possible to check this point directly as the speed of rotation cannot be independently varied. However, the cell speed does change with the number of stages in the build, and in the two-, three- and four-stage compressors, where it was possible to monitor the shape of the cell, no deviation from an axial profile was observed. If, on the other hand, the structure of the cell was more like that of a dead wake, the cell would have assumed an obvious helical twist at the speeds found, and the angle of this twist would have altered from build to build.

The concept of an active cell structure is thus supported in most respects by the experimental results, and the sketch given in Fig. 14 can therefore be regarded as a reasonable model of the flow in the compressor. It should be emphasized that, although multi-stage data have been used to study and discuss the cell structure, the concept of an active cell, and the fundamental idea of mass transfer across the cell due to the physical influence of the rotor blades moving through the retarded flow, is applicable even for a single-stage machine or rotor alone. Fundamental to this model is the basic idea that the stalled blades behave like paddle wheels, sweeping the flow in their direction of motion, and not at all in the manner of unstalled aerofoils.

4.2 Axial movement of fluid in stall cell

The description of the cell structure given in the previous section was predominantly concerned with flow in the tangential direction. It can be seen from the experimental results, however, that, although small by comparison with the tangential flow, a certain amount of fluid does move axially through the blade rows. This axial movement may manifest itself as either a net flow towards the front or back of the compressor, or else as a recirculation within the blade rows themselves.

The axial movement of fluid through a stall cell is most easily studied by considering the flow direction measurements in the plane behind the rotor. The flow there has a much smaller tangential component and the measured angles therefore provide a clearer indication of the sense of the flow. The appropriate measurements at a radial position towards the outer wall for the three-stage builds are given in Fig. 4, where it can be seen that the details of the flow in each build are different. To assist with the interpretation of these measurements, a sketch is provided in Fig. 15 showing the flow patterns in the intermediate ϕ^* build. Although this sketch is only a two-dimensional view of a highly complex three-dimensional situation, it can be seen that the stall cell may be divided into two parts: one in which the flow has an axial component of velocity towards the front of the compressor (i.e. reversed flow) and the other in which the axial component of the flow is towards the rear of the compressor (i.e. through-flow).

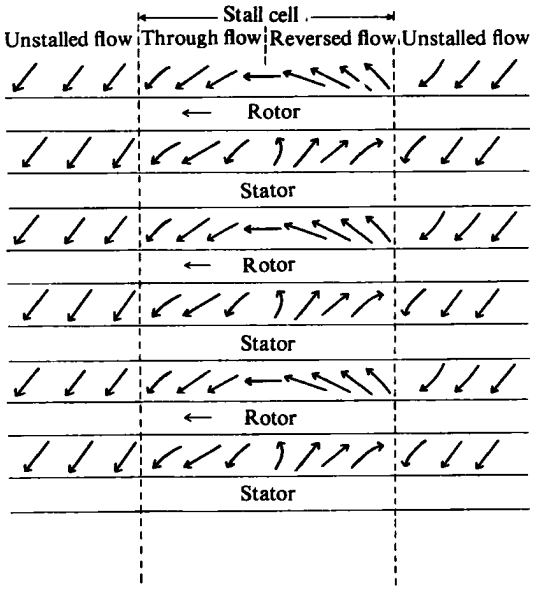

Fig. 15. Pictorial sketch of stalled flow in a three-stage compressor of intermediate ϕ^* build

In the intermediate ϕ^* build, the areas of the reversed and through-flow appear to be of roughly equal proportions, but the measurements of Fig. 4 indicate that this is not true for the other two builds. The low ϕ^* compressor shows a complete absence of reversed flow, while in the high ϕ^* build the measurements suggest that the flow is reversed over almost the entire cell. In terms of through-flow and reversed flow, the situation in the three compressor builds can be summarized by the sketches in Fig. 16. These sketches are only representative of conditions in the multi-stage builds, since the details of the flow may differ in a single-stage build.

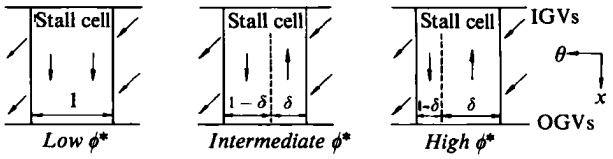

Fig. 16. Sketch showing variation in axial drift through stall cells for different values of design flow coefficient, ϕ^*

If a mean axial velocity component is assumed for each of the various parts of the flow field, then a simple continuity equation can be written to express the net flow through the annulus in any of the compressor builds. Consider first the low ϕ^* compressor, for which there was found to be no reversed flow in the stall cell. Approximate values of the local flow coefficient, $\phi = C_x/\bar{U}$, deduced from the velocity measurements, are +0.1 in the stall cell and 0.35 in the unstalled flow. It may then be shown, and confirmed by independent measurement of stall cell size, that for the low ϕ^* compressor the stall cell covers the entire annulus at an area average flow coefficient, $\bar{\phi}$, equal to 0.1, i.e. before the flow drops to zero.

In the case of the high ϕ^* compressor, about 85 per cent of the cell has a reversed axial flow (i.e. $\lambda = 0.85$), and appropriate values of local flow coefficient are ± 0.2 in the stall cell (+ being the forward and − the backward flow) and 1.15 in the unstalled flow. This leads to a prediction, again confirmed by independent measurement, that the stall cell will only cover 90 per cent of the annulus at shut-off, i.e. at $\bar{\phi} = 0$.

The two examples considered here provide some idea of the possible order of magnitude of the axial drift through the stall cell and can be used to show how the sense of the net drift, either positive or negative, can influence the overall behaviour of the compressor. In the low ϕ^* build, where the stall cell reaches maximum size at a positive flow rate, rotating stall is replaced by axisymmetric stall with an accompanying change in the characteristic in Fig. 2. Alternatively, in the high ϕ^* build, rotating stall is still present at $\bar{\phi} = 0$, and so that characteristic shows no obvious change in behaviour as the flow rate approaches zero.

With regard to the general question of axial drift in models of the stalled region, it will be recalled that Dunham (**12**) assumed positive flow in the stall cell. However, McKenzie (**13**) and, more recently, Day *et al.* (**10**) assumed zero flow, and Gray (**14**) negative flow. From the above discussion, it is clear that these assumptions are based on an over-simplified concept of the cell as, in reality, both positive and negative flow can coexist in the stalled region.

Fig. 17 shows sketches to assist with the visual interpretation of the measured flow patterns in the radial direction at the circumferential centre of the cell for the low and high ϕ^* machines. In the low ϕ^* build, the flow pattern is strongly three-dimensional, and shows movement of fluid in both the positive and negative x directions. Part of the flow entering the rotor at the hub moves through the blade row and emerges from the trailing edge plane with a comparatively low velocity and in a direction which is predominantly tangential, i.e. at 70° or 80° to axial. The remainder of the flow entering the rotor is centrifuged outwards, at the same time acquiring a very high velocity in the whirl direction. This centrifuged fluid leaves the blade row on the upstream side with a small component of axial velocity in the negative direction (100° to downstream axial) and, after interacting with any blade row ahead of the rotor (either stator or IGV), it may well re-enter the rotor in a recirculatory fashion. It should be stressed, however, that the velocities in the tangential direction are much greater than those in the meridional plane shown here, and therefore a particular fluid particle may only complete a fraction of the cyclic process in the time it takes for the particle to move from one side of the cell to the other.

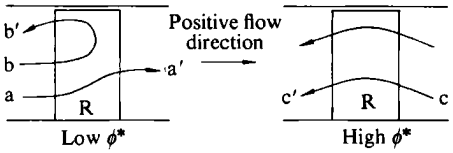

Fig. 17. Sketch comparing radial flow patterns for different design flow coefficients, ϕ^*

In the high ϕ^* build, the flow is more two-dimensional in nature and moves consistently in the reversed flow direction, i.e. negative C_x. The fluid entering the rotor does so at a very oblique angle, as in the absolute reference frame it is moving in the tangential direction opposite to that of the rotor (250° to downstream axial) with a velocity that is sometimes as high as $0.7\bar{U}$. This is illustrated by the sketch in Fig. 18, drawn from results shown in Figs 8 and 9. The flow entering the rotor from behind thus has a relative velocity approaching $1.7\bar{U}$. The

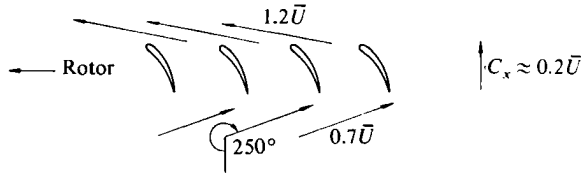

Fig. 18. Sketch of velocity vectors in stall cell into and out of rotor for high ϕ^* compressors

losses during the actual entry process must be very large and the flow cannot be considered in normal unstalled aerofoil terms, but once the fluid emerges from the upstream side of the blade row it has acquired an absolute velocity, mainly in the tangential direction, well in excess of that of the blades themselves and sometimes as high as $1.5\bar{U}$. It is only with the existence of a net flow in the reversed direction that these exceedingly high velocities ahead of the rotor can be explained.

Some heuristic explanations can be given for the differences in the flow patterns for the two extreme values of ϕ^*. If flow is imagined to leave the rotor on the upstream side, it does so with a large whirl component and a small axial component. This flow impinges on the trailing edges of the upstream blades and, as already noted, the behaviour of rotor or stator blades in the stall cell should be visualized as stalled plates or as paddle wheels rather than normal unstalled aerofoils. The low ϕ^* blades have a trailing edge inclination 40° to the axial, and flow endeavouring to move upstream will tend to be deflected tangentially. The high ϕ^* blades are inclined so that their trailing edges point in the axial direction and more of the flow is likely to be captured and directed upstream. It is noteworthy that both high and low reaction stages (in either case, one blade row is highly staggered) present blade trailing edge angles likely to inhibit the axial flow in the upstream direction even for quite large design flow coefficients.

4.3 Torque measurement and energy dissipation

The torque characteristics for the three-stage builds of the low and high ϕ^* compressors are shown in Fig. 19. During unstalled operation, it is to be expected that the torque levels in these two machines will be different, owing to the difference in the pressure rise and mass flow. Near the shut-off point, however, where the overall pressure rise produced by the two builds is roughly equal (Fig. 2), the sustained high level of the torque in the high ϕ^* build can only be explained in terms of greater energy dissipation in the stall cell.

The picture of the cell structure given in Fig. 14, where the axial drift in the stall cell is neglected, suggests that the fraction of the total torque attributable to the stalled part of the flow could be calculated solely from the momentum changes that occur at the edges of the cell, since, under ideal conditions, the flow in the centre of the cell would require very little work to keep it moving in the tangential direction. In reality, however, the axial movement of the fluid in the cell (either because of meridional recirculation or net axial drift) leads to interaction between the rotor and stator rows. The amount of energy dissipated, and hence the torque, depends upon the precise details of the flow in the stall cell. To explain why the torque measurements indicate greater losses in the case of the high ϕ^*

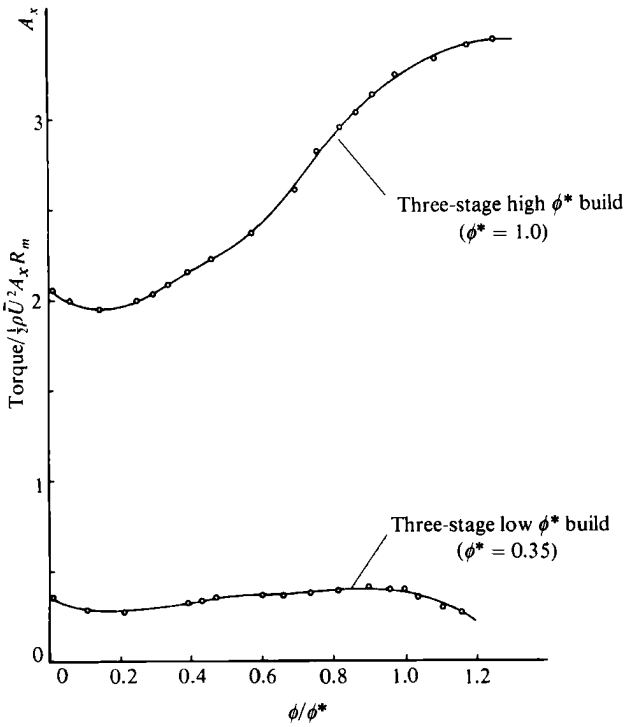

Fig. 19. Comparison of torque measurements in two compressors of different design

build than in the low ϕ^* build, the details of the flow in these two compressor builds should be examined more carefully.

In the case of the low ϕ^* compressor, some of the fluid entering the rotor at the hub drifts axially through the rotor (line a–a′, Fig. 17), while the remainder experiences recirculation in the meridional plane (line b–b′). The mass flow rate of the fluid which passes through the rotor is comparatively small and, as the velocity and flow direction are found to change little in crossing the blade row (Fig. 8), the energy absorbed by this fluid is thought to be insignificant. In the case of the recirculating fluid, on the other hand, the velocity changes that occur are considerably larger. The measurements in Fig. 8 show fluid entering the rotor near the hub with a tangential component of velocity of about $0.5\bar{U}$, and leaving the rotor at the tip with a tangential velocity approaching that of blade speed $\bar{U}$. The net change in whirl velocity undergone by the recirculating fluid is therefore equal to $0.5\bar{U}$.

It is impossible to estimate the mass flow rate of the fluid involved in this recirculatory process for the low ϕ^* compressor, and therefore no momentum change calculations can be made. The high ϕ^* compressor build provides a more interesting opportunity to study the energy interchange between rotor and stalled fluid because some numerical calculations are possible based on simple mass flow estimates. It will be recalled that the flow in this build is fairly uniform radially, and that the greater part of the cell, about 85 per cent, is occupied by reversed flow (line c–c′, Fig. 17). The reversed flow passing through the rotor in the absolute frame of reference is shown in Fig. 18.

Taking the flow direction ahead of the rotor to be more or less tangential, the change in the tangential component of velocity which occurs as the flow passes through the high ϕ^* rotor is given by

$$\Delta C_\theta \approx 1.2\bar{U} - (0.7\bar{U}\sin 250°)$$
$$\approx 1.85\bar{U}$$

The value of ΔC_θ in this build is almost four times as great as that in the low ϕ^* build.

For the sake of simplicity, the torque will be calculated at the point where the stall cell covers the entire annulus, and it will also be assumed that the entire annulus area is occupied by reversed flow. It has been shown that this will be true over only 85 per cent of the stalled region in this build, but for the present purposes this assumption is not considered unreasonable. The mass flow rate of the fluid drifting through the annulus can then be calculated from the mean axial velocity coefficient, which the velocity measurements suggest to be of the order of $0.2\bar{U}$. The mass flow rate is therfore $\dot{m} = \rho A_x (0.2\bar{U})$, where A_x is the cross-sectional area of the compressor annulus.

The fluid undergoes a change in tangential velocity of $1.85\ \bar{U}$, as shown above, and so for a three-stage compressor the net torque is given by

$$\tau = 3(\dot{m}\Delta C_\theta R_m)$$
$$= 3(\rho \times A_x \times 0.2\bar{U} \times 1.85\bar{U} \times R_m)$$

where R_m is the mean radius of the compressor. This torque can be non-dimensionalized by a reference value $\frac{1}{2}\rho\bar{U}^2A_xR_m$, so that

$$\frac{\tau}{\frac{1}{2}\rho\bar{U}^2A_xR_m} = 2.2$$

This estimate compares very favourably with the measured value at shut off for the high ϕ^* machine shown in Fig. 19.

Having considered the part played by the rotor blades in putting energy into the stalled flow, the role of the stator blades in dissipating this energy should now be considered. The sketches in Fig. 17, used to illustrate the flow patterns in the stall cell, show that in both compressor builds the high-velocity fluid leaving the rotor tips has a small negative axial velocity, and therefore impinges at a very oblique angle on the trailing edges of the blades in the upstream stator row. It is these oblique angles, and the consequent separation and mixing, that is thought to bring about the dissipation of the mechanical energy in the flow with a consequent temperature rise in the compressor.

The idea that the energy in the fast-moving fluid ahead of the rotor is lost, rather than converted to useful pressure, is supported by the observation that the regions of high total pressure in the cell are strictly limited to the areas ahead of the rotor rows. This pressure is not convected into the spaces ahead of the stators or into the unstalled flow surrounding the cell, as can be seen from the measurements in Fig. 5.

Although no temperature measurements were taken in the present tests, it was obvious when working on the test rig that the stalled temperature rise in the high ϕ^* build was far greater than that in the low ϕ^* build.

4.4 Pressure fluctuations during stall

The presence of very high tangential velocities ahead of the rotors in the stall cell has been noted many times in the preceding work. These tangential velocities give rise to

centrifugal accelerations which must be balanced by radial gradients in static pressure. The resulting difference in pressure between the inner and outer walls can be estimated from the simple radial equilibrium equation:

$$p_{tip} - p_{hub} = \int_{hub}^{tip} \rho \frac{C_\theta^2}{R} dR$$

where R is the radius at any point between the inner and outer wall, and C_θ is the corresponding tangential component of velocity in the stall cell. The variation in C_θ from hub to tip at the circumferential centre of the stall cell in the three-stage compressor builds can be obtained from the velocity measurements shown in Fig. 8.

In Table 3, the static pressure differences estimated from the radial equilibrium using measured values of C_θ are compared with those obtained from Fig. 10. In each case, the comparisons are made for the flow ahead of the first rotor.

Table 3

Compressor build	From radial equilibrium $(p_{tip} - p_{hub})/\frac{1}{2}\rho\bar{U}^2$	From Fig. 10 $(p_{tip} - p_{hub})/\frac{1}{2}\rho\bar{U}^2$
Low ϕ^*	0.17	0.34
Intermediate ϕ^*	0.25	0.48
High ϕ^*	0.43	0.47

In the unstalled flow surrounding the cell, the radial variation in static pressure is of the order of 0.06 $(\frac{1}{2}\rho\bar{U}^2)$ for all three builds, in every case very much less than that in the cell.

In keeping with the fact that the tangential velocities increase with compressor design flow rate (Fig. 8), the static pressure differences in both columns can be seen to increase with ϕ^*. The values of p based on the radial equilibrium equation are, however, lower in all three cases than the values suggested by the static pressure in Fig. 10. The discrepancies between the two columns suggest that centrifugal effects in the tangential plane are not the only factors causing the radial pressure gradients in the stall cell. Curvature of the streamlines in the meridional plane, or even radial flow itself, may also be contributory factors. In this respect it is interesting to note that the difference between the values of p in the two columns is largest in the case of the low ϕ^* build, where the flow is strongly three-dimensional, and smallest in the case of the high ϕ^* build, where the flow is more or less uniform across the height of the annulus.

In spite of the differences between the two columns, it is clear that centrifugal effects in the swirling flow ahead of the rotor account for the greater part of the radial pressure gradient in the stall cell. This observation is important in view of the fact that the only stall theory to take any account of the centrifugal effects in the stall cell is that of Fabri (3), and the centrifugal effects considered there are those due to the 'solid-body' rotation of the 'dead' cell as a whole, taking no account of the movement of the fluid within the cell. It is also important because it shows that the rotor and stator rows will perform differently in stalled flow; the former is moving in the absolute reference frame and the latter is not. Thus, even for a high hub–tip ratio compressor, such as the ones used here with a ratio of 0.8, the character of the stalled flow is dominated by radial effects.

The average static pressure in the unstalled part of the flow ahead of the first rotor will be approximately equal to $p_o - \frac{1}{2}\rho C^2$, where p_0 is atmospheric pressure and C is the local velocity of the unstalled flow ahead of the first rotor. Since the velocity upstream of the rotor increases with design flow coefficient, it is to be expected that the static pressure in the unstalled flow will decrease markedly as ϕ^* increases. This expectation is borne out by the measurements in Fig. 6. The level of the pressure in the stall cell, on the other hand, is above atmospheric and roughly the same in each case. A possible explanation for this last observation can be found by examining the flow in the stalled part of the annulus ahead of the first rotor.

In Fig. 10 it is seen that, for the low ϕ^* compressor build, the radial pressure distribution in the stall cell ahead of the first rotor is centred about atmospheric pressure. This point was more clearly illustrated when the inner and outer wall static pressures for this build were traced through the compressor inlet as far as the plane ahead of the first rotor. It was found that, in contrast with the unstalled flow, the pressure at the circumferential centre of the stall cell remains approximately equal to atmospheric pressure right up to the rotor inlet. This is attributed to the fact that in a large stall cell, covering a third of the annulus or more, the flow in the area ahead of the cell is almost stagnant and so the static pressure in this region will be atmospheric. (The pressures due to unsteady effects in the inlet flow are small by comparison with the pressures being considered and, therefore, need not be taken into account. In any case, it can be shown by a small perturbation analysis that measurements such as these, taken at the circumferential centre of the cell, will not be influenced by the pressure fluctuations due to the unsteadiness of the flow.)

In cases where strong reversed flow is absent, it is therefore suggested that the level of the static pressure in the stall cell ahead of the first rotor should be such that the integral of the pressure over the height of the cell will be equal to atmospheric pressure. When reversed flow is present, however, atmospheric pressure cannot be assumed in the compressor inlet, and allowance must be made for the resulting increase in static pressure. Indeed, for the intermediate and high ϕ^* builds, where reversed flow is stronger, it can be seen from Fig. 10 that the mean pressure level in the stall cell in these two builds is above atmospheric.

It follows from these ideas that, if the mean static pressure in the stall cell ahead of the first rotor is approximately atmospheric, the static pressure recorded on the outer wall in the stalled region will be above atmospheric pressure by an amount roughly equal to half the difference in pressure between hub and tip, i.e. by $\frac{1}{2}(p_{tip} - p_{hub})$. This is confirmed by the measurements in Fig. 6. Ahead of the rotor, the outer-wall static pressure at the centre of the stall cell increases as the design flow coefficient, ϕ^*, is raised, which is consistent with the size of $(p_{tip} - p_{hub})$ rising with ϕ^*, as noted above.

From the outer-wall static measurements in Fig. 6, it can also be seen that strong circumferential pressure

gradients exist between the stalled and unstalled parts of the flow, especially in the high ϕ^* build. These pressure gradients must play a part in the circumferential movement of fluid in the stall cell, accelerating and decelerating the flow circumferentially in an unsteady manner as the stall cell passes. The circumferential static pressure gradients diminish towards the rear of the compressor, because the pressure in the unstalled flow rises rapidly and in the stalled flow only very slowly, yet the velocity and flow direction measurements show that the general behaviour of the flow in the last stage of the compressor is the same as that in the first. This is a perplexing aspect of the flow which has not yet been resolved.

4.5 Details of unstalled flow

Whereas the discussion so far has centred on the details of the flow in the stall cell, certain significant aspects of the flow in the unstalled part of the annulus are also revealed by the present measurements.

It will be recalled from the literature that the parallel compressor models of stalled flow all make the assumption that the unstalled part of the annulus behaves as it would under steady, unstalled, axisymmetric conditions, and that the flow coefficient in this region will be such as to ensure that the unstalled delivery static pressure in the exit plane is the same as that for the stalled flow.

To investigate this point, it is helpful to consider the specific example of the three-stage intermediate ϕ^* build. The total-to-static characteristic for this build is shown in Fig. 20, along with the axial velocity recorded at mid-blade height behind the first rotor. The velocity trace was taken at a mean flow coefficient of $\bar{\phi} = 0.33$ and, therefore, a horizontal line has been drawn through the point, B, on the stalled branch of the characteristic corresponding to this flow coefficient. The line can be seen to intersect the unstalled curve at A, which, according to the parallel compressor model, will be the operating point of the unstalled part of the annulus. The flow coefficient at A is 0.56, which compares favourably with the value of 0.57 measured with the hot-wire. Similar measurements in other builds have confirmed the accuracy of the parallel compressor model in predicting flow coefficients in the unstalled flow.

From the total-to-static characteristic in Fig. 20*a*, it may be deduced in the normal way, i.e. by assuming zero axial flow in the cell, that the fraction of the annulus stalled is equal to 41 per cent. This is in reasonable agreement with the value of 39 per cent estimated from the velocity recordings shown in Fig. 20*b*. The assumption of zero flow in the stall cell would have introduced some small error for the low or high ϕ^* builds because of the net positive and negative flows observed in the stall cell.

The parallel compressor model makes the implicit assumption that the velocity in the unstalled part of the annulus is constant and independent of the size of the stall cell. While this is true over the greater part of the operating range, it can be seen from the measurements in Fig. 7 that the unstalled velocity actually decreases as the stall cell size increases. This effect was found to be more pronounced in the high θ^* case. The true situation in the stall cell is obviously more complicated than that assumed by the parallel compressor model. Nevertheless, the above example shows that this model can be used as a working hypothesis to provide reasonable results.

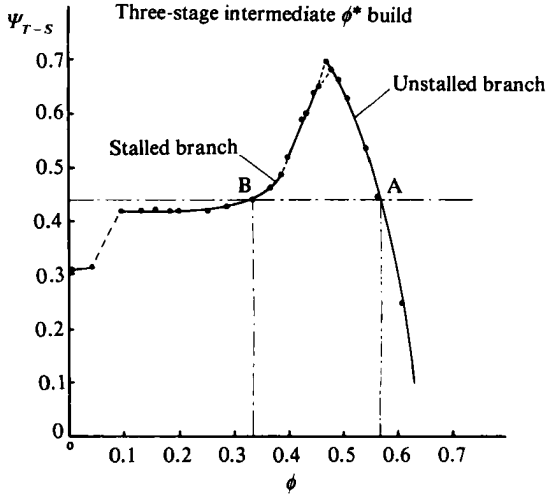

Fig. 20*a*. Compressor characteristic showing operating point at which measurements below were obtained

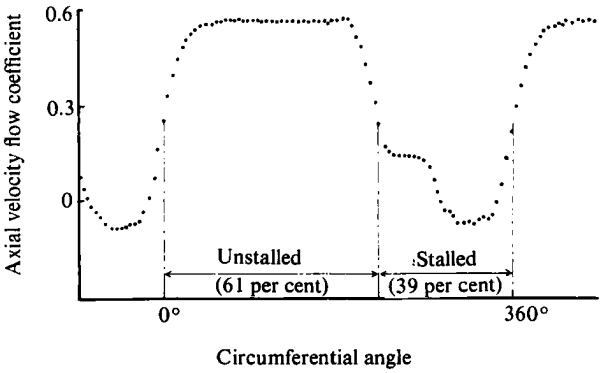

Fig. 20*b*. Velocity measurement at a flow coefficient of 0.33

5 CONCLUSIONS

On the basis of the results described here the following conclusions are possible.

In terms of cell structure, it has been established that the edges of the cell within the blade rows of the compressor do not follow streamlines in the unstalled flow, and therefore the customary idea of the cell as a dead wake cannot be correct. Instead, it has been shown that unstalled flow crosses tangentially from one side of the cell to the other, thus giving rise to the concept of an active rather than a passive type of structure.

The tangential movement of the fluid in the cell is ascribed to the influence of the rotor blades which, when stalled, behave as paddle wheels, dragging the flow circumferentially around the annulus. The stator blades within the cell behave likewise as stationary paddle wheels. The flow in the rotor differs because the fluid in the rotor blade passages tends to be centrifuged radially outward. This simple picture of blade behaviour in stalled flow explains the general similarity of the flow patterns observed in compressors of so many design configurations, from isolated rotors to multi-stage builds. It also permits an explanation of why the flow patterns in a multi-stage rig are repeated stage-by-stage through the compressor, instead of the latter stages operating in the wake of a disturbance attached to the first stage. The flow can, of course, only repeat if the compressor is axially well-

matched, which is not generally true of high-speed machines off design.

In spite of the general similarity between the stalled flow patterns in all compressor builds, it was found that the finer details of the flow are affected by the stagger angle of the blades (that is to say, the design flow rate, ϕ^*) and the number of stages in the compressor. In the latter respect, it was concluded that, although the flow in a single-stage build shows similarities with that in a multistage configuration of the same blading, the finer details of the flow are sufficiently different to preclude the extrapolation of single-stage data to multi-stage configurations.

In all compressor builds, it was found that the flow in the stall cell is characterized by high velocities ahead of the rotor and low velocities behind. Fluid trapped in the stalled rotor blade passages always appears to drift out of the blade row on the upstream side, giving rise to the observed high velocities in the area ahead of the rotor. (No definitive explanation for the direction of this drift can be given.) This fast-moving fluid is brought to rest by the stator blades, during which process most of its kinetic energy is dissipated, in the form of losses, with a resulting temperature rise. Because of this interaction, it is possible for a stalled compressor to absorb almost as much torque as an unstalled compressor.

Although the compressor used in the tests was of high hub–tip ratio, 0.8, it was found that the flow in the stall cell is highly three-dimensional, especially during full-span stall.

It has been observed that the flow in a part-span stall cell is much like that in a full-span cell. (Two unexplained exceptions to this were noted, however. These occurred in single-stage builds of high flow rate and showed a combination of rotating stall associated with the rotor and axisymmetric wall-stall associated with the stator, Day (**9**).)

It was concluded that centrifugal effects distinguish the rotor rows from the stator rows, thereby dispelling the traditional notion that the stall cell should rotate at 50 per cent of the rotor speed in order to preserve symmetry between rotor and stator performance during stall. No further observations were made on the subject of cell speed, except that the speed of rotation of full-span stall cells increases rapidly with the number of stages in the compressor (Table 2), and that cell structure appears unaffected by the cell speed.

Centrifugal effects in the stalled flow ahead of the rotor blades are responsible for strong radial gradients in static pressure, and are also thought to contribute to the increase in static pressure which occurs ahead of each rotor in the stalled parts of the compressor.

By noting the repeatability of cell structure through the compressor and attributing the overall pressure rise in the stall cell to the influence of centrifugal effects in the swirling flow ahead of the rotor, some explanation is provided for the observation that the total-to-static pressure rise per stage appears to be the same for all compressors, i.e. independent of the details of blading used. This observation was first made McKenzie (**13**) and is supported by the model of compressor behaviour described by Day *et al.* (**10**).

The circumferential static pressure gradients between the stalled and unstalled parts of the flow can be very large. Even though the pressure gradients are reduced towards the rear of the compressor, the flow in the last stage of a stalled multi-stage compressor behaves very much like that in the first stage.

It is observed that the assumption of irrotational flow immediately ahead of the rotor is not justified. This is because the circumferential swirl in this region is found to accompany the intense disturbance within the stall cell, whether it is full-span or only part-span. Potential flow theory cannot, therefore, be used to describe the inlet condition around the annulus after the inception and growth of small disturbances.

The often used analytic assumption that the flow in the stalled blade passages is merely reduced below normal by boundary layer separation is a gross over-simplification of the real situation. Recirculation under the influence of centrifugal effects, or even net reversed flow, is more probable than a simple reduction in the local flow rate.

In view of the significance of centrifugal effects in the rotor blade passages, it appears that the perturbation analyses which take no account of these effects may be more applicable to stationary rather than moving blade rows.

6 ACKNOWLEDGEMENTS

The authors wish to thank Derby College of Arts and Technology for the loan of the test compressor and the Ministry of Defence (Procurement Executive) for supporting the work.

APPENDIX

REFERENCES

(1) TAKATA, H. and NAGANO, S. 'Non-linear analysis of rotating stall', *A.S.M.E.* 1972, Paper No. 72-GT-3.
(2) STENNING, A. H. and KRIEBEL, A. R. 'Stall propagation in a cascade of aerofoils', *Trans. A.S.M.S.* 1958 **80**, 777.
(3) FABRI, J. 'Rotating stall in axial flow compressors', Symposium on turbomachinery, Cambridge 1967. Published by I.Mech.E. in *Internal aerodynamics (turbomachinery)* 1970.
(4) DUNHAM, J. 'Observations of stall cells in a single stage compressor', *A.R.C. CP 584* 1961.
(5) BODEEN, C. A. *Vector velocity fluctuations of propagating stall in axial flow compressors* Thesis, California Institute of Technology, 1961.
(6) PAVLENKO, G. V. Work review by Yershov, V. N. 'Unstable conditions of turbodynamics. Rotating stall'. Translated by the Foreign Technology Division of the U.S.A., reference FTD-MT-24-04-71. Source: 'Neustoychivyye reshimy turbomachin', Urashchayushchiysya Sryv, Moscow, Izd-vo Mashinostroyeniye, 1966.
(7) TANAKA, S. and MURATA, S. 'On the partial flow rate performance of axial flow compressor and rotating stall. Second report: influences of impeller load and a study of the mechanism of unstable performances', *Bulletin of J.S.M.E.* 1977 **18**, (No. 117).
(8) DAY, I. J. 'Detailed flow measurements during deep stall in axial flow compressors', Paper presented at AGARD meeting held in Monterey, California, September 1975.
(9) DAY, I. J. *Axial compressor stall* Ph.D. Dissertation, University of Cambridge, 1976.
(10) DAY, I. J., GREITZER, E. M. and CRUMPSTY, N. A. 'Predictions of compressor performance in rotating stall', *Trans. A.S.M.E., J. Engng Pwr* 1978 **100** (No. 1).
(11) RANNIE, W. D. 'The axial compressor stage', Chapter F, *Aerodynamics of turbines and compressors* 1964, Ed. W. R. Hawthorne, Vol. **X** of Princeton Series (Oxford University Press).
(12) DUNHAM, J. *Non-axisymmetric flows in axial compressors* I.Mech.E. Monograph No. 3, October 1964.
(13) McKENZIE, A. B. Private communication, 1973.
(14) GRAY, S. Private comments, 1973.